Polymer 51 (2010) 469–474

Contents lists available at ScienceDirect

Polymer

journal homepage: www.elsevier.com/locate/polymer

Clay nanocomposites based on poly(vinylidene fluoride-co-hexafluoropropylene): Structure and properties

Antonios Kelarakis*, Suren Hayrapetyan, Seema Ansari, Jason Fang, Luis Estevez, Emmanuel P. Giannelis*

Department of Materials Science and Engineering, Cornell University, Ithaca, NY 14853, USA

ARTICLE INFO

Article history:
Received 14 September 2009
Received in revised form
20 November 2009
Accepted 28 November 2009
Available online 2 December 2009

Keywords:
Clay nanocomposite
PVDF copolymer
Toughness

ABSTRACT

Structure-properties relationships in poly(vinylidene fluoride-co-hexafluoropropylene), PVDF-HFP, clay nanocomposites are reported for the first time. Addition of organically modified clays to PVDF-HFP promotes an α to β transformation of the polymer crystals. The degree of transformation depends on the nature of the clay surface modifier and scales with the strength of the interactions between the clay and the polymer. The nanocomposites exhibit significant increases in elongation to failure compared to the neat copolymer. In addition, their dielectric permittivity is higher over a wide temperature range. Their mechanical and dielectric properties scale similar to the amount of the β phase present in the nanocomposites.

1. Introduction

The nanoscopic origin of the macroscopic properties in polymer-clay nanocomposites has been the subject of intense investigations which have been summarized in a number of reviews [1–6]. One of the key points to the development of this class of hybrid materials is the realization that the native inorganic ions within clay cavities can be replaced by bulkier ammonium ions linked to hydrocarbon chains. This pretreatment can significantly alter the thermodynamics of host/guest interactions, facilitating polymer intercalation within the clay galleries and giving rise to intercalated or exfoliated mesostructures. These clay hybrids often exhibit attractive performance enhancements with respect to thermomechanical properties, dimensional stability, barrier characteristics and flame retardancy. Suffice to say that those enhanced properties carry a great promise for a wide range of technological applications.

Conceptually, a number of structural changes induced by nanoparticles can be expressed in terms of mobility confinement of the polymer chains in the vicinity of the organic/inorganic interface. In that sense, clay nanocomposites can serve as model systems to study polymer dynamics under severe confinement as in the case of ultrathin films or fluids in restricted environments [7]. The interfacial structure and dynamics influence, in turn, the macroscopic properties of the nanocomposites so that performance improvements can be directly related to the dispersion state of the filler, the total area of the internal interfaces and to the strength of matrix–nanoparticle interactions.

Due to their rigid nature, clay platelets can function as nucleating agents that are able to modify the crystallization behavior of the polymer matrix [8]. However, martensitic-like transformations of the crystalline phase have been observed only in selected polymer-clay combinations. The most well explored examples of this type are the development of γ phase in Nylon 6 at the expense of the α phase in the neat polymer [9,10] and the evolution of β phase instead of the α form in Poly(vinylidene fluoride), PVDF [11–21]. The latter has a considerable impact in applications where pyroelectric, piezoelectric, ferroelectric or magnetostrictive response is desirable [22]. The all-trans configuration of β phase imparts a high dipole moment (7.0×10^{-30} Cm/repeat unit) due to the alignment of the polar C–F bonds perpendicular to the polymer axis chain.

Introducing other monomer units to the PVDF backbone generates a family of copolymers that exhibit certain advantages compared to the homopolymer such as enhanced piezoelectricity and improved mechanical behavior [23–26]. Due to their properties PVDF copolymers are considered ideal candidates for several applications including electroacoustic and electromechanical convertors, actuators, ferroelectric memory devices, mechatronics and artificial muscles. In this study, we report for the first time on structure-properties relationships in a series of clay nanocomposites based on poly(vinylidene fluoride-co-hexafluoropropylene), PVDF-HFP. In particular, we correlate the role of

* Corresponding authors.
E-mail addresses: ak385@cornell.edu (A. Kelarakis), epg2@cornell.edu (E.P. Giannelis).

0032-3861/$ – see front matter © 2009 Elsevier Ltd. All rights reserved.
doi:10.1016/j.polymer.2009.11.057

clay surface modification on the crystallization behavior of the polymer matrix, the morphology of the nanocomposite and the macroscopic response of the hybrids materials with respect to their rheological, mechanical and dielectric properties.

2. Experimental

2.1. Materials

Poly(vinylidene fluoride-co-hexafluoropropylene) referred hereafter as PVDF-HFP is a random copolymer (6% HFP comonomer) purchased from Aldrich in pellet form and was ground to fine powder before further use.

Three commercial organically modified montmorillonites (MMT) clays were used; I.30T from Nanocor Inc., which is octadecyltrimethyl ammoniun-substituted MMT (MMT-Alk), Cloisite 30B from Southern Clay Products, a bis(hydroxyethyl)methyl tallow ammoniun-exchanged MMT (MMT-OH), and Perchem 97 from Southern Clay Products that is modified with benzyltallowdimethylammonium (MMT-Ar). The unmodified montmorillonite (MMT-Na^+) was provided by Southern Clay Products. All clays were repeatedly washed in ethanol-water to remove any excess ammonium ions before use.

2.2. Sample preparation

Prior to nanocomposites preparation, both clays and polymer were dried in a vacuum oven for several hours. The components were first thoroughly mixed in a Flack-Tek DAC-150 FV speed mixer, before being melt coextruded by means of a laboratory scale DSM twin screw microcompounder at 215 °C under flowing nitrogen for 4 min. Specimens with ring (diameter 25.2 mm, thickness 1.5 mm) or dumbbell (gauge length 29.5 mm, width 4.0 mm, thickness 1.6 mm) shape were prepared by a Daca Instruments microinjector with the barrel at 260 °C, the mold at 90 °C and the injection pressure at 690 kPa. For comparison, unfilled copolymer samples were treated in an identical fashion.

For the co-precipitation method, 5 wt% PVDF-HFP solution in *N*,*N*-dimethyl formamide, (DMF, Sigma Aldrich) was mixed with the appropriate amount of 2 wt% MMT-Ar in DMF (that had been subjected to vigorous stirring overnight at elevated temperature followed by ultrasonication for 2 h). The mixture was then stirred overnight and ultrasonicated for another 2 h. The ternary solution was then coagulated by adding water as antisolvent and the precipitated material was dried under vacuum for 4 days at 70 °C to form a nanocomposite abbreviated as MMT-Ar/DMF. Ring specimens (diameter 25.4 mm, thickness 1.6 mm) were prepared by compression molding at $T = 210$ °C and 20 MPa pressure for 10 min and then were left to crystallize at room temperature.

3. Methods

Wide-angle, X-ray diffraction (WAXS) spectra were recorded at room temperature using a Scintag Inc. θ-θ goniometer (CuKα radiation, $\lambda = 1.54$ Å). Transmission electron microscopy (TEM) imaging was performed on FEI Tecnai T12 using microtomed ultrathin samples. Scanning electron microscopy (SEM) images of fracture surfaces were taken on a KECK FE-SEM, LEO 1550. Differential scanning calorimetry (DSC) thermographs were collected on a TA Instrument Q1000 series calorimeter over the temperature range −50 to 150 °C at a scan rate of 10 °C/min. Tensile tests were performed at room temperature with an Instron 5500 Mechanical Tester at constant strain rate of 5 mm/min.

Rheological measurements were performed on a Paar Physica Modular Compact Rheometer 300 (MCR 300) equipped with parallel plate geometry (diameter 25 mm). Measurements were performed in small amplitude oscillatory shear, at a fixed temperature 240 °C, in a dry nitrogen atmosphere to suppress oxidative degradation. The frequency scans covered a range from 0.1 to 600 s^{-1}. Dielectric properties were recorded using a Novacontrol GmbH broadband dielectric spectrometer in the temperature range −100 to 150 °C.

4. Results and discussion

The d-spacing increase in all XRD patterns of the PVDF-HFP nanocomposites compared to the neat clays (Fig. 1) provides clear evidence of polymer intercalation in the silicate layers. The d-spacing for MMT-Alk is 28 Å while MMT-OH and MMT-Ar show marginally lower values. The XRD trace of the nanocomposite prepared by co-precipitation (MMT-Ar/DMF in Fig. 1) shows close similarities with the XRD pattern of the melt-extruded analogue. No intercalation was observed when the pristine (Na^+-form) clay was used. A representative TEM image of the nanocomposites is shown in Fig. 2 suggesting a uniform dispersion of clay tactoids. The intercalated mesostructures observed for the clay nanocomposites based on the organically modified clays imply the presence of favorable matrix–filler interactions that promotes the development of extensive organic/inorganic interfaces. The alignment of clay tactoids seen in Fig. 2 results from the unidirectional shear field present during molding.

At higher q values, the diffraction pattern of the neat copolymer (Fig. 3) can be indexed as the crystal planes of the monoclinic unit cell of the α phase of PVDF [18]. The copolymer shows the same structural motifs as the homopolymer (i.e. α phase) but the presence of bulky HFP comonomer units results in a decrease in crystallinity. Incorporation of organically modified clay nanoparticles to PVDF-HFP matrix leads to the evolution of a new reflection peak β(200)/β(110) at $2\theta = 21°$, characteristic of the orthorhombic unit cell of β phase of PVDF analogous to what was observed previously for the homopolymer. Clearly, the amount of the β phase in the nanocomposite depends on the type of clay used with MMT-Alk < MMT-OH < MMT-Ar. The clay induced crystal transformation was further confirmed by FTIR spectroscopy (Fig. 4). The α-phase peaks centered at 763 and 796 cm^{-1} are clearly observed only for the neat polymer while the β-phase peak at 840 cm^{-1} can only be seen in the nanocomposite. TEM images shown in Fig. 5 reveal pronounced morphological variations due to the nucleation efficacy of nanoclays. Interestingly, while the neat polymer forms well

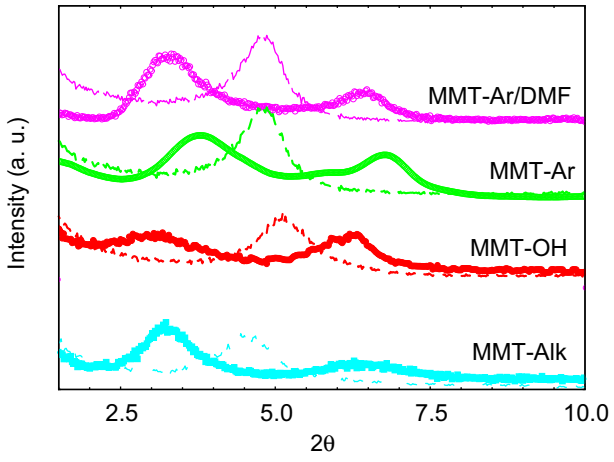

Fig. 1. XRD patterns of PVDF-HFP clay nanocomposites (clay content 5 wt%) compared to the corresponding neat nanoclays (dashed lines).

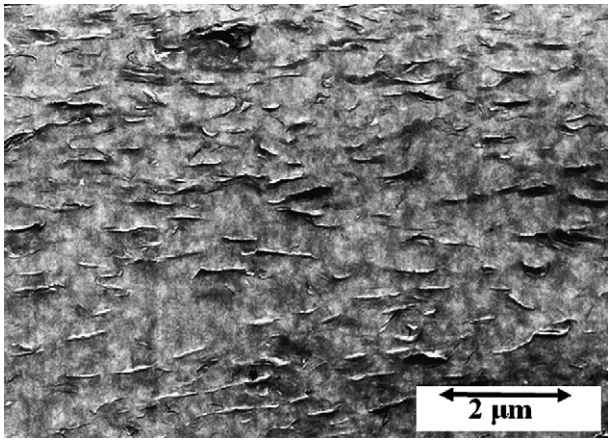

Fig. 2. TEM image of a PVDF-HFP based nanocomposite containing 5 wt% MMT-Ar.

defined spherulites with radii in the order of several micrometers, those superstructures are not detected in the presence of organoclays.

The rich polymorphism of PVDF and PVDF based copolymers (forming five distinct phases namely α,β,γ,δ,ε) originates in large from the very similar van der Waals volume of fluorine compared to hydrogen atom that allows high symmetry and provides flexibility to the polymer chain. The stabilization of the β phase in PVDF induced by clay nanoparticles has been originally related to the spatial confinement of the polymer chains imposed by the rigid nanofillers [11]. It has been suggested that crystallization of PVDF under constrained conditions favors the evolution of β phase, in a manner similar to that observed in binary immiscible blends containing PVDF droplets as the minor component [27]. Alternatively, a mechanism analogous to that developed for the epitaxial crystallization of β modification on KBr substrate has been proposed [28]. This mechanism highlights the geometrical similarities between the crystal lattice of the inorganic phase (KBr, clay) and the β phase of PVDF [14,29]. It should be noted that the β phase is favored in the presence of Ag nanoparticles [30], functionalized multiwall carbon nanotubes [31] and functionalized graphene sheets [32]. Alternatively stress can induce a transformation from α to β phase, even in the absence of clay, as shown in Fig. 3 taken across the tensile fractured surface of neat PVDF-HFP copolymer (diffractogram noted as "stretched" in Fig. 3). The uniaxial or biaxial deformation of PVDF and PVDF copolymers in the temperature range between the glass transition and the melting point of the

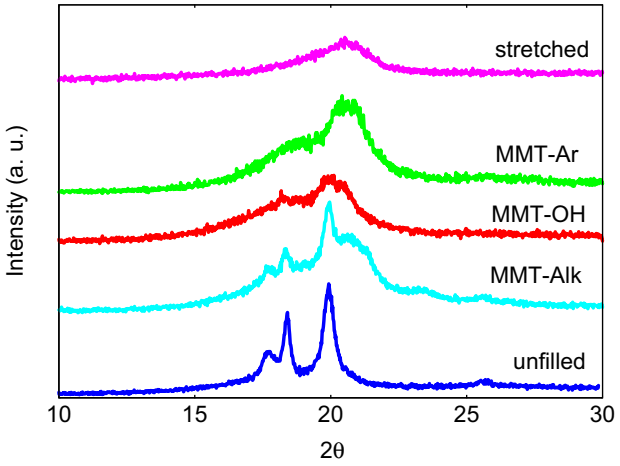

Fig. 3. Crystalline reflections of PVDF-HFP and 5 wt% clay based nanocomposites.

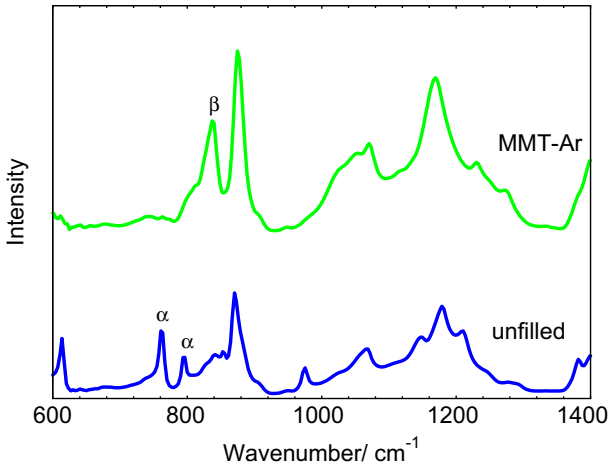

Fig. 4. FTIR spectra of neat PVDF-HFP copolymer (bottom) and a nanocomposite containing 5 wt% MMT-Ar (top). The characteristics frequencies for α and β phases are shown in the spectra.

polymer in the absence or presence of electric field is a widely applied technique for the preparation of the β phase [33–35].

DSC thermographs (second heating cycle) of various nanocomposites are compared with the neat polymer in Fig. 6. The addition of MNT-Na^+ does not affect the melting point of the copolymer T_m = 157 °C. In contrast, addition and dispersion of organically modified clays to the polymer matrix leads to higher T_m.

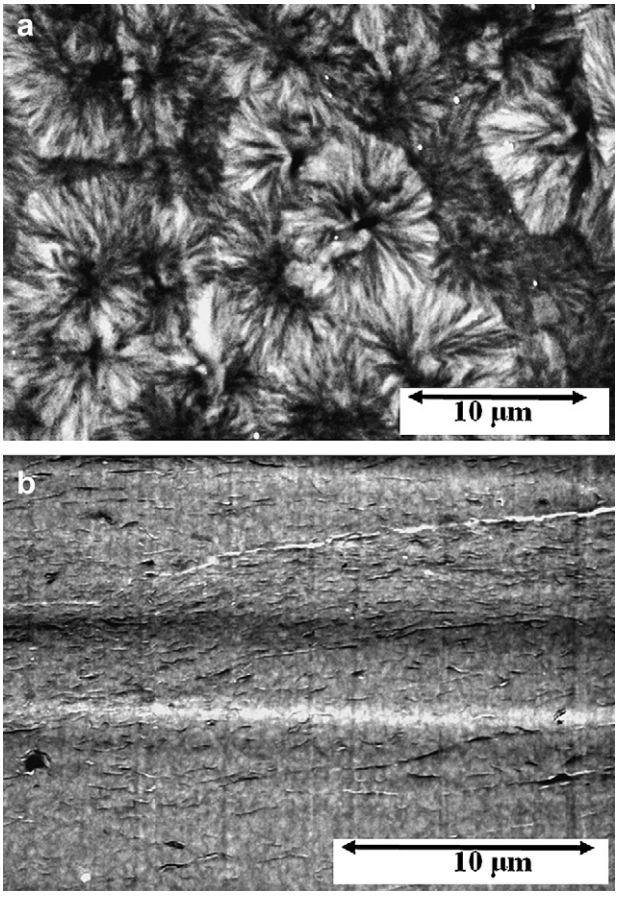

Fig. 5. TEM images of; a) neat copolymer showing well defined spherulites and b) 5 wt% MMT-Ar nanocomposite.

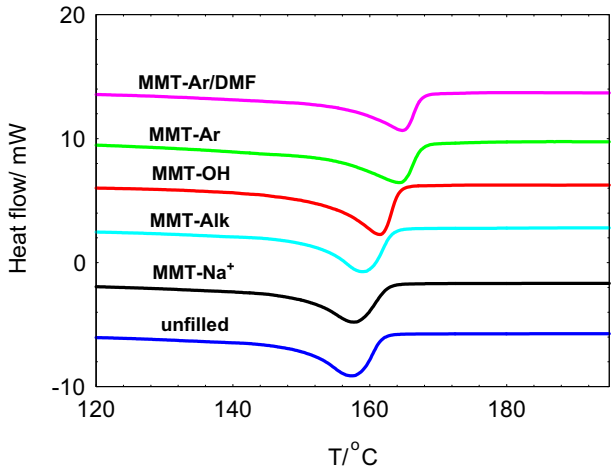

Fig. 6. DSC thermographs (second heating cycle) of various PVDF-HFP clay nanocomposites (clay content 5 wt%).

In particular, the melting points of MMT-Alk, MMT-OH and MMT-Ar filled hybrids were found to be 159,161 and 165 °C, respectively. The increase of T_m in the nanocomposites scales with the amount of β phase present, as a direct consequence of the enhanced thermal stability of β crystals.

The stress–strain plots for the PVDF-HFP copolymer and nanocomposites are shown in Fig. 7. The elongation at break increases from 20% for the neat copolymer to approximately 110 and 130% for MMT-OH and MMT-Ar hybrids respectively, without any adverse effect on Young modulus. In contrast, the MMT-Alk nanocomposite exhibits only a modest increase in strain to break, while the unmodified MMT hybrid shows the same maximum strain as the unfilled sample. Overall, the toughness (defined as the area under the stress/strain curve) of the MMT-Alk, MMT-OH and MMT-Ar nanocomposites exhibit 2,5 and 6 fold increase respectively compared to the unfilled counterpart. We note that the trend in increasing toughness is consistent with the amount of β phase present.

Enhancements in toughness have been reported for a limited number of clay based nanocomposite systems including PVDF [14] and PVDF based blends [36]. In general, nanofillers homogeneously dispersed in a polymer matrix, in addition to inducing changes in crystallinity (both degree and type of phase) can give rise to a percolated network that has a protective role against the onset of catastrophic cracking; the load transfer efficiency largely depends upon the interfacial nanofiller/polymer shear stress [37].

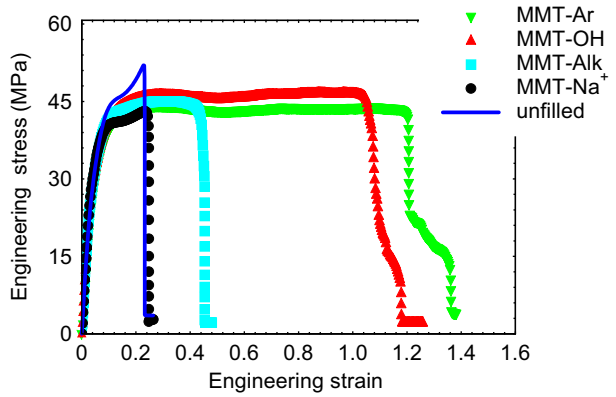

Fig. 7. Uniaxial (tensile) deformation plots of PVDF-HFP copolymer and clay nanocomposites (clay content 5 wt%) performed at room temperature and deformation rate of 5 mm/min.

The SEM image of the tensile fractured cross-section of MMT-Ar hybrid is shown in Fig. 8. The SEM image essentially demonstrates the architectural features of a super tough surface that can effectively direct and distribute the load during uniaxial deformation. Specifically, we note the organization of the polymer matrix into fiber-like conformations and superstructures oriented parallel to the stretching direction. In rubbery matrices, the realignment of the clay particles themselves along the stretching direction effectively blocks crack propagation and deflection [38,39].

In an effort to better understand the mechanical response we studied the viscoelastic response of the nanocomposites and the neat polymer using isothermal ($T = 240$ °C) frequency scans (Fig. 9). The rheological behavior of the neat polymer corresponds to an entangled polymer melt having a short relaxation time. The introduction of MMT-Na^+ leaves the rheological signature essentially unaffected. In contrast, profound deviations of the ideal melt behavior, mainly in the low frequency limit, can be observed for the organoclay based nanocomposites. This behavior is typical for several classes of hybrid materials and has been attributed to the formation of a physically cross-linked superstructure due to the presence of the nanofillers [40–44]. Essentially, the development of such a physical network tends to increase the relaxation time of the melt. At high frequencies the viscoelastic spectra of nanocomposites are not as sensitive to the presence of nanofillers. This behavior indicates that nanoclays have a bigger effect on the long-range rather than the short-range motions of the polymer.

The dielectric response for the neat copolymer and nanocomposites is shown in Fig. 10. Three major processes are typically seen for such copolymers [45–47]. A β relaxation around −40 °C due to the glass transition of the amorphous phase, a relaxation of the crystalline phase above 0 °C and an order–disorder transition of the ordered ferroelectric phase at even higher temperatures. The crystalline transition virtually disappears in systems where the polar β phase dominates. The dielectric response at low temperatures (0 °C) seems to be insensitive to the presence of the clay. In contrast, the clay affects significantly the response at high temperatures. The dielectric response at high temperatures is affected by a number of processes including mobility of ionic carriers, and development of space charges and polarization in the amorphous phase. Upon heating, the combined action of those effects gives rise to a steep increase of dielectric permittivity, even in the absence of clay. This steep increase is more dramatic for the nanocomposites and it commences at much lower temperatures. Interestingly, the increase is consistent with the trend seen before (i.e. nanocomposites with higher β phase content exhibit higher values of ε′, consistent with the increased polarity of the β phase).

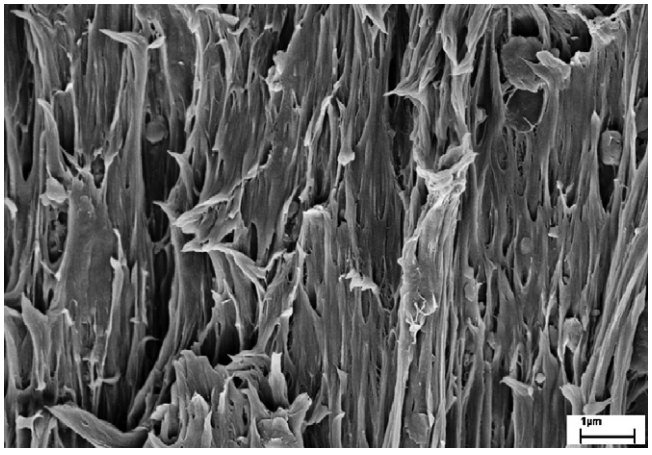

Fig. 8. SEM image of the fractured surface of 5 wt% MMT-Ar nanocomposite.

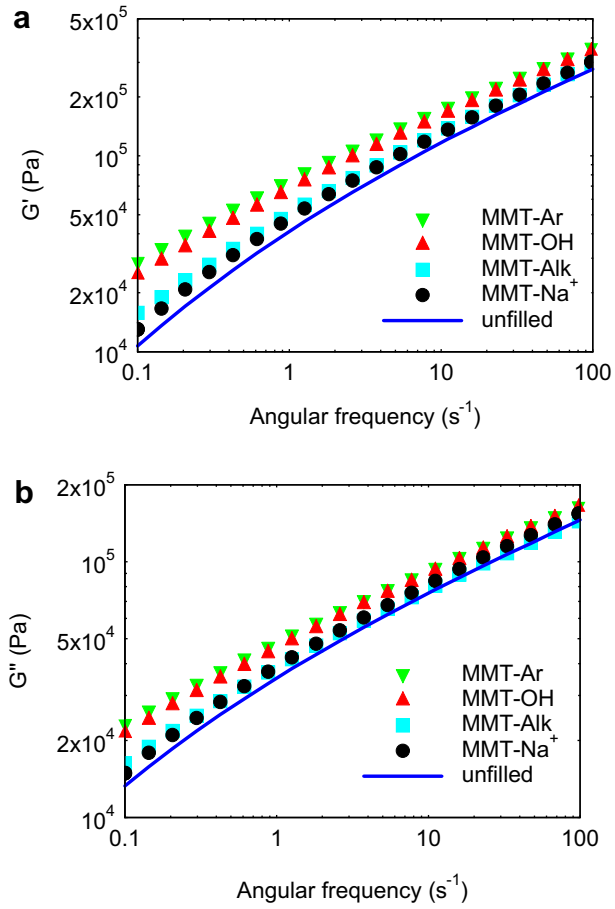

Fig. 9. Frequency dependence of; a) storage (G′) and b) loss (G″) modulus of PVDF-HFP based nanocomposites containing 5 wt% clay; MMT-Na^+ (circles), MMT-Alk (squares), MMT-OH (upwards triangles), MMT-Ar (downwards triangles), solid lines refer to neat polymer. ($T = 240$ °C).

A remarkable correlation exists between the structural features and the macroscopic properties of the nanocomposites. Recall that the amount of β phase in the nanocomposites increases in the order MMT < MMT-Alk< MMT-OH < MMT-Ar. Significantly, the elongation to break, the dielectric permittivity and the complex viscosity of the nanocomposites appear to follow the same trend. The minimal impact of the MMT-Na^+ clay on the properties can be attributed to the lack of compatibility with the polymer. Of the organoclays MMT-Alk interacts the least with the copolymer due to the lack of any significant chemical interactions of the aliphatic surfactant with PVDF-HFP. On the other hand, hydrogen bonding between the hydroxyl groups of MMT-OH and the electronegative fluorine of PVDF-HFP can give rise to strong polymer-clay interactions. The substantial reinforcement observed for MNT-Ar nanocomposites can be attributed to the favorable energetics between the polarizable aromatic rings with the C–F as well as C–H bonds [48,49]. Based on *ab initio* calculations, the interaction energies for benzene complexes with methane and fluoromethane were estimated 1.5 and 4.2 kcal/mole, respectively and have been attributed to dispersion (long-range) rather than charge transfer contributions [49]. Those values can be compared with the hydrogen bridging energy in the water dimer estimated at about 5 kcal/mol [50].

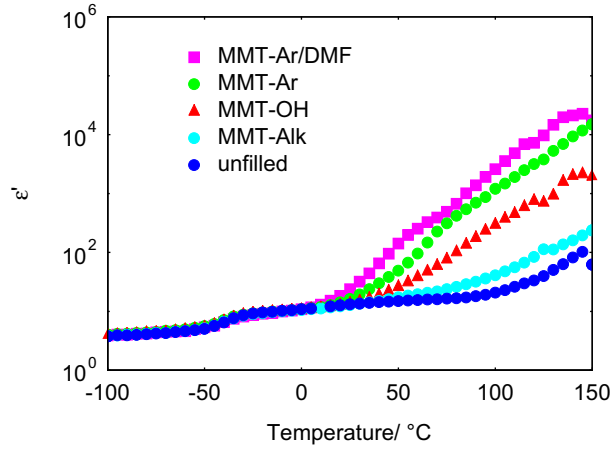

Fig. 10. Real part of dielectric permittivity of several PVDF-HFP nanocomposites (clay content 5 wt%) as a function of temperature at frequency 1 Hz.

5. Conclusions

Addition of organically modified clays to PVDF-HFP copolymer promotes an α to β transformation of the polymer crystals. The degree of transformation depends on the nature of the clay surface modifier and scales with the strength of the interactions between the clay and the polymer. The nanocomposites exhibit significant increases in elongation to failure compared to the neat copolymer. In addition, their dielectric permittivity is higher over a wide temperature range. A remarkable correlation exists between their structure and macroscopic properties. Their mechanical and dielectric properties correlate extremely well with the amount of the β phase present in the nanocomposites and can be fine-tuned by controlling the strength of the interactions between the polymer and the nanoparticles.

Acknowledgements

E.P. Giannelis acknowledges the support of Award No. KUS-C1-018-02, made by King Abdullah University of Science and Technology (KAUST).

References

[1] Giannelis EP. Adv Mater 1996;8:29–35.
[2] Ray SS, Okamoto M. Prog Polym Sci 2003;28:1539–641.
[3] Okada A, Usuki A. Macromol Mater Eng 2006;291:1449–76.
[4] Paul DR, Robeson LM. Polymer 2008;49:3187–204.
[5] Pavlidou S, Papaspyrides CD. Prog Polym Sci 2008;33:1119–98.
[6] Camargo PHC, Satyanarayana KG, Wypch F. Mater Res 2009;12:1–39.
[7] Anastasiadis SH, Karatasos K, Vlachos G, Manias E, Giannelis EP. Phys Rev Lett 2000;84:915–8.
[8] Jog JP. Mater Sci Technol 2006;22:797–806.
[9] Medellin-Rodriguez FJ, Burger C, Hsiao BS, Chu B, Vaia R, Phillip S. Polymer 2001;42:9015–23.
[10] Maiti P, Okamoto M. Macromol Mater Eng 2003;288:440–5.
[11] Priya L, Jog JP. J Polym Sci Polym Phys 2002;40:1682–9.
[12] Priya L, Jog JP. J Appl Polym Sci 2003;89:2036–40.
[13] Priya L, Jog JP. J Polym Sci Polym Phys 2003;41:31–8.
[14] Shah D, Maiti P, Gunn E, Schmidt DF, Jiang DD, Batt CA, et al. Adv Mater 2004;16:1173–7.
[15] White JL, Kim Y. J Appl Polym Sci 2004;92:1061–71.
[16] Pramoda KP, Mohamed A, Phang IY, Liu T. Polym Int 2005;54:226–32.
[17] Dillon DR, Tenneti KK, Li CY, Ko FK, Sics I, Hsiao BS. Polymer 2006;47:1678–88.
[18] Buckley J, Cebe P, Cherdack D, Crawford J, Ince BS, Jenkins M, et al. Polymer 2006;47:2411–22.
[19] Patro TU, Mhalgi MV, Khakhar DV, Misra A. Polymer 2008;49:3486–99.
[20] Yu W, Zhao Z, Zheng W, Song Y, Li B, Long B, et al. Mater Lett 2008;62:747–50.
[21] Wu T, Xie T, Yang G. J Polym Sci Part B Polym Phys 2009;47:903–11.
[22] Lovinger AJ. Science 1983;220:1115–21.
[23] Neese B, Wang Y, Chu B, Ren K, Liu S, Zhang QM, et al. Appl Phys Lett 2007;90:242917.
[24] Zhou X, Zhao X, Suo Z, Zou C, Runt J, Liu S, et al. Appl Phys Lett 2009;94:162901.
[25] Zhang QM, Bharti V, Zhao X. Science 1998;280:2101–4.

[26] Xu H, Cheng ZY, Olson D, Mai T, Zhang QM, Kavarnos G. Appl Phys Lett 2001;78:2360–2.
[27] Yang X, Kong X, Tan S, Li G, Ling W, Zhou E. Polym Int 2000;49:1525–8.
[28] Lovinger AJ. Polymer 1981;22:412–3.
[29] Yamada E, Nishioka A, Suzuki H, Koda T, Ikeda S. Jpn J Appl Phys 2007;46:7371–4.
[30] Manna S, Batabyal SK, Nandi AK. J Phys Chem B 2006;110:12318–26.
[31] Manna S, Nandi AK. J Phys Chem C 2007;111:14670–80.
[32] Ansari S, Giannelis EP. J Polym Sci Part B Polym Phys 2009;47:888–97.
[33] Lando JB, Olf HG, Peterlin A. J Polym Sci 1966;4:941–51.
[34] McGrath JC, Ward IM. Polymer 1980;21:855–7.
[35] Sajkiewicz P, Wasiak A, Goclowski Z. Eur Polym J 1999;35:423–9.
[36] Kelarakis A, Giannelis EP, Yoon K. Polymer 2007;48:7567–72.
[37] Kelarakis A, Yoon K, Sics I, Somani RH, Hsiao BS, Chu B. Polymer 2005;46:5103–17.
[38] Gersappe D. Phys Rev Lett 2002;89:058301.
[39] Shah D, Maiti P, Jiang DD, Batt CA, Giannelis EP. Adv Mater 2005;17:525–8.
[40] Xu W, Raychowdhury S, Jiang DD, Retsos H, Giannelis EP. Small 2008;5:662–9.
[41] Krishnamoorti R, Giannelis EP. Macromolecules 1997;30:4097–102.
[42] Krishnamoorti R, Yurekli K. Curr Opin Colloid Interface Sci 2001;6:464–70.
[43] Kelarakis A, Yoon K, Somani RH, Chen X, Hsiao BS, Chu B. Polymer 2005;46:11591–9.
[44] Bhattacharya SN, Kamal MR, Gupta RK. Polymeric nanocomposites: theory and practice. Munich: Hanser; 2007 [chapter 4].
[45] Cebe T, Grubb DT. Macromolecules 1984;17:1374–84.
[46] Kochervinskii VV, Malyshkina IA, Markin GV, Gavrilova ND, Bessonova NP. J Appl Polym Sci 2007;105:1101–17.
[47] Lu Y, Claude J, Norena-Franco LE, Wang Q. J Phys Chem B 2008;112:10411–6.
[48] Lu YX, Zou JW, Wang YH, Yu QS. Chem Phys 2007;334:1–7.
[49] Tsuzuki S, Honda K, Uchimaru T, Mikami M, Tanabe K. J Phys Chem A 2002;106:4423–8.
[50] Feyereisen MW, Feller D, Dixin DA. J Phys Chem 1996;100:2993–7.